Tellus (2003), 55B, 498–511
Printed in UK. All rights reserved

TELLUS
ISSN 0280–6509

Sensitivity of optimal extension of CO_2 observation networks to model transport

By PRABIR K. PATRA[1]*, SHAMIL MAKSYUTOV[1] and TRANSCOM-3 MODELERS[2], [1]*Frontier Research System for Global Change, Yokohama 236 0001, Japan;* [2]*D. Baker, P. Bousquet, L. Bruhwiler, Y-H. Chen, P. Ciais, A. S. Denning, S. Fan, I. Y. Fung, M. Gloor, K. R. Gurney, M. Heimann, K. Higuchi, J. John, R. M. Law, T. Maki, P. Peylin, M. Prather, B. Pak, P. J. Rayner, J. L. Sarmiento, S. Taguchi, T. Takahashi and C-W. Yuen*

(Manuscript received 2 January 2002; in final form 9 December 2002)

ABSTRACT

Optimal extensions of the surface CO_2 observation network have been determined using 15 global transport models and a time-independent inverse model. The regional average CO_2 flux estimate uncertainty is minimized based on the TransCom-3 (level 1) framework. An ensemble model calculation shows that the regional average CO_2 flux uncertainties could be reduced to about 0.36, 0.32, 0.28 or 0.26 Gt C yr^{-1} per region, from about 0.53 Gt C yr^{-1} per region corresponding to the basic network, after adding 5, 10, 15 or 20 optimally located stations, respectively. The additional station locations are mostly found in continental South America and Africa. The distribution of the efficiency in estimation of flux uncertainty reduction per station tends to become more uniform with the extension of the network. We show that the multimodel approach to network design converges if a large enough extension is considered; about 20 stations in this inverse model framework. The reduction in the flux uncertainty for the first few stations depends on the model of atmospheric transport, and is nearly proportional to the simulated signal from local emissions in the surface layer. In addition, it is seen that the simulated spatial and temporal variability of CO_2 concentration has significant influence on the distribution of the additional stations as well as determining the regional flux estimate uncertainty.

1. Introduction

Fluxes of CO_2 from the earth's surface have traditionally been estimated from atmospheric observations of CO_2 and carbon isotopes (e.g. Tans et al., 1990; Francey et al., 1995; Ciais et al., 1995). Later, the regional distributions of CO_2 sources/sinks at continental scale were also targeted, but with somewhat less success (Fan et al., 1998; Bousquet et al., 1999; Gurney et al., 2002). Generally, fluxes from a large fraction of regions cannot be estimated with a high degree of confidence. This arises from the uneven distribution and restricted number of atmospheric observations available worldwide (GLOBALVIEW, 2000). Many areas of land are not covered by measurements, which leaves the surface source estimations for those regions underdetermined in atmospheric data inversion studies. Such a lack of observations in certain regions could also influence the estimation of fluxes from other regions where measurements are available. The estimation of fluxes is dependent on the model simulation of CO_2 transport and the resolution at which the surface fluxes are to be estimated by the inverse model (Gurney et al., 2002; Kaminski et al., 2001).

As stated above, CO_2 sources and sinks for different geographic regions are estimated by using information from atmospheric observations and global transport model simulations. The inversion technique is described in detail elsewhere (e.g. Tarantola, 1987; Enting et al., 1993). To achieve better inverse model performance, it is desirable to model atmospheric transport as accurately as possible and construct an efficient enhancement of the network of atmospheric

*Corresponding author.
e-mail: prabir@jamstec.go.jp

measurements. The extension of the CO_2 measuring network to obtain maximum constraint on inverse model results was studied only recently (Rayner et al., 1996; Gloor et al., 1999; 2000; Patra and Maksyutov, 2002). We focus our attention on an optimal extension of the existing CO_2 measuring network by using simulations from 15 models participating in TransCom-3. The use of a statistically significant number of transport models will allow us to propose an optimal network for surface CO_2 observations that is less dependent on model transport and with a higher level of confidence.

Simulated annealing (SA) is commonly used in various types of network design and was also employed in earlier studies on optimal sampling of atmospheric CO_2 for improving performance of surface source inversion (Rayner et al., 1996; Gloor et al., 2000). This technique, however, is computationally expensive and probabilistic by design. More recently an alternative approach for optimal network design, Incremental Optimization (IO), has been introduced (Patra and Maksyutov, 2002). Although the theoretical basis of IO is not so well evolved as compared to SA, the practical implementation of IO is simple and unambiguous. This characteristic of IO often leads to a better network optimization of surface CO_2 observation (Patra and Maksyutov, 2002). By using this method the proposed station locations under study can be ranked based on their positive influence on the flux estimate uncertainty reduction, which will be discussed later. Since IO is computationally very efficient, we use this method to conduct different types of network design experiments with several transport model simulations.

In Section 2 we briefly describe the materials and methods used here. Results and discussion will be presented in Section 3. The main conclusions are summarized in Section 4.

2. Materials and methods

2.1. Bayesian inversion

Assuming linearity of the forward transport problem, the source strengths are predicted by the least-squares solution of the equation $GS = D$, where D and S are the atmospheric CO_2 data and surface fluxes, respectively, and G represents the model transport (Tarantola, 1987). In Bayesian synthesis inversion (Enting et al., 1993), the following function is minimized to reduce the mismatches between the atmospheric observations and predicted responses, and the a priori sources (S_0) and predicted sources:

$$\left[(S - S_0)C_{S_0}^{-1}(S - S_0)^T\right] + \left[(GS - D)C_D^{-1}(GS - D)^T)\right]. \quad (1)$$

Here C_D and C_S denote the error covariances associated with atmospheric CO_2 data and surface fluxes, respectively. The parameters S and C_S, pertaining to a set of subdivided regions of the globe, will be optimized to match the global distribution of CO_2 through the inversion. The solution of eq. (1) is (see Section 1.7 in Tarantola, 1987 for details):

$$\langle S\rangle = S_0 + \left(G^T C_D^{-1} G + C_{S_0}^{-1}\right)^{-1} \times G^T C_D^{-1}(D - GS_0) \quad (2)$$

and the predicted flux covariances are given by

$$C_S = \left(G^T C_D^{-1} G + C_{S_0}^{-1}\right)^{-1}. \quad (3)$$

Our aim is to minimize $\Sigma_i C_S(i, i)$ with model calculated G and C_D at the CO_2 observation sites. According to eq. (3), the estimated source uncertainty is strongly determined by the CO_2 data variability C_D and simulated source signal G. The absolute estimation of C_D from the location specific data variability has always been difficult, both from observations and theory (Masarie and Tans, 1995; Gloor et al., 2000). This parameter is supplied as a combined measure of our ability to observe atmospheric CO_2 at high accuracy and to simulate the observations using global transport models. The procedure for how to estimate C_D for the new measurement stations is described in Section 2.2. It is similar to the one utilised in an earlier study (Patra and Maksyutov, 2002). The inverse of the matrix $(G^T C_D^{-1} G + C_{S_0}^{-1})$ is determined by singular value decomposition (SVD). The SVD of a matrix A is factorization of form $U\lambda V^T$, where the columns of U (left singular matrix) and V (right singular matrix) are orthogonal, and λ is a diagonal matrix containing the singular values (Press et al., 1992).

2.2. Atmospheric data and model simulations

We use the GlobalView-CO_2 data (GLOBALVIEW, 2000) over 115 locations to create the 'basic set' of atmospheric data. Secondly, *a priori* knowledge of the surface fluxes (S_0) and uncertainties (C_{S_0}) associated with a set of subdivided regions of the globe are taken from the TransCom-3 protocol (Gurney et al., 2002;

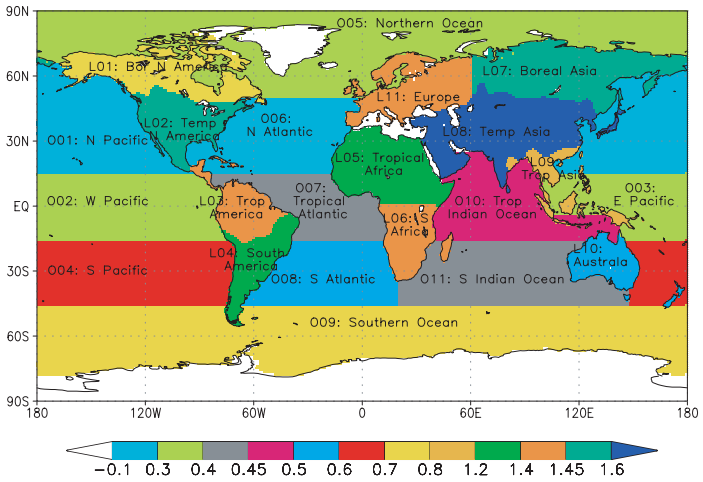

Fig. 1. TransCom-3 divided land and ocean regions (11 each) of the world. The colour bar indicates the prior flux uncertainty associated with each region. The whitened areas are not considered in the inverse model.

2003). Figure 1 shows the names and locations of land and ocean regions for which the S_0 and C_{S_0} are prescribed in the TransCom-3 inversion. Finally, responses for different flux types and regions are simulated using 15 global atmospheric transport models (see Table 1 for gross model configurations). The model responses are sampled at measurement sites to form the sensitivity matrix G. The inverse modeling framework is identical to that described in the TransCom-3 experimental protocol (see Gurney et al., 2003 for details). It considers four presubtracted emission maps, namely, for fossil fuels (1990 and 1995 scenario), neutral biosphere and the oceans. In addition, there are 11 terrestrial and 11 oceanic carbon

Table 1. *List of the global transport models participating in TransCom-3 project*[a]

SL no.	Model name[b]	Winds	Resolution (lat × long)	Vertical layers
1.	UCB	GISS GCM-II	4.0° × 5.0°	9
2.	UCI	GISS GCM-II	4.0° × 5.0°	9
3.	UCI:s	GISS GCM-II	4.0° × 5.0°	23
4.	UCI:b	GISS GCM-II	4.0° × 5.0°	9
5.	JMA	JMA GCM	2.5° × 2.5°	32
6.	MATCH:CCM3	NCAR CCM3	2.8° × 2.8°	28
7.	MATCH:NCEP	NCEP 1990	2.8° × 2.8°	28
8.	MATCH:MACCM2	MACCM2	5.6° × 2.8°	24
9.	NIES:FRSGC	ECMWF 1997	2.5° × 2.5°	15
10.	NIRE:CTM-96	ECMWF 1995	2.5° × 2.5°	15
11.	RPN:SEF	GCM Online	2.8° × 2.8°	27
12.	SKYHI	GCM Online	3.0° × 3.6°	40
13.	TM2	ECMWF 1990	7.5° × 7.5°	9
14.	TM3	ECMWF 1990	4.0° × 5.0°	19
15.	CSU	GCM Online	4.0° × 5.0°	17
16.	GCTM[c]	ZODIAC GCM	2.4° × 2.4°	11

[a]The basic meteorology used in the simulation as well as the horizontal and vertical resolutions of the models are also given (see Gurney et al., 2003 for further details).
[b]First part denote the primary model names and the last part is to indicate the model variants, as appropriate.
[c]The GCTM model (no. 16) because this work was started before that model simulation become available.

basis function flux maps, which are to be adjusted by inverse calculation.

Note that the predicted values of C_S do not depend on D but require a fair estimation of C_D [eq. (3)]. The analyses of atmospheric data errors have been made with different models of the residual CO_2 concentration variability or residual standard deviations (RSDs): one for the GlobalView station network (observed) and another for the set of candidate sites (modelled). The elements of C_D for the candidate sites are calculated from the high-frequency model outputs assuming that these are primarily caused by the synoptic-scale atmospheric transport. We used the daily output of NIES (National Institute for Environmental Studies, Tsukuba)/FRSGC global transport model (Maksyutov and Inoue, 2000) for the combined CO_2 sources from fossil fuel combustion, the oceans and net ecosystem production. The residuals are calculated by fitting the CO_2 seasonal cycle with a low-pass filter (Nakazawa et al., 1997). As is seen from Fig. 2, the match between the modeled and 'observed' RSDs varies between good (South China Sea cruise) and poor (middle and high latitudes in the Northern Hemisphere). The over-prediction of the variability at Northern Hemisphere stations in the model could be due to sampling protocol differences between the model and the observation network. Measurements were made potentially sampling background (usually oceanic) air, thus significantly reducing the influence of nearby sources in coastal sites. However, we do not see this as a major problem for our analysis as long as most of our proposed stations target continental signals, assuming that those have to be observed regardless of the high temporal variability.

2.3. *Incremental optimization algorithm*

The algorithm used in Patra and Maksyutov (2002) divides the optimization problem into several subproblems and is referred to as Incremental Optimization (IO). We begin with a 'basic set' (see Fig. 3d, open diamonds), containing the measured values of D and C_D at 115 GlobalView locations and a set of 446 candidate stations, selected from the meteorological stations presently operating around the globe. At the first iteration subproblems are constructed by adding one of the candidate stations to the 'basic set' and the inverse calculation is performed on 446 data combinations containing 116 stations. The data combination that results in the greatest reduction in the average source estimate uncertainty for an individual model or averaged over 15 transport models (ensemble case) is added to the 'basic set', and the newly introduced station is removed from the list of candidate stations. In the second step the next set of subproblems is constructed by adding remaining 445 candidate stations to the new basic set. Thus the 'basic set' grows in size, and the other set reduces. The process is continued until the reduction of flux uncertainty due to a new station become negligible.

3. Results and discussion

In this section, we will show the optimal network extension based on response functions from the 15 TransCom-3 participating models for the sources described in Section 2.2. We have used them both separately and in combination as an ensemble in this work.

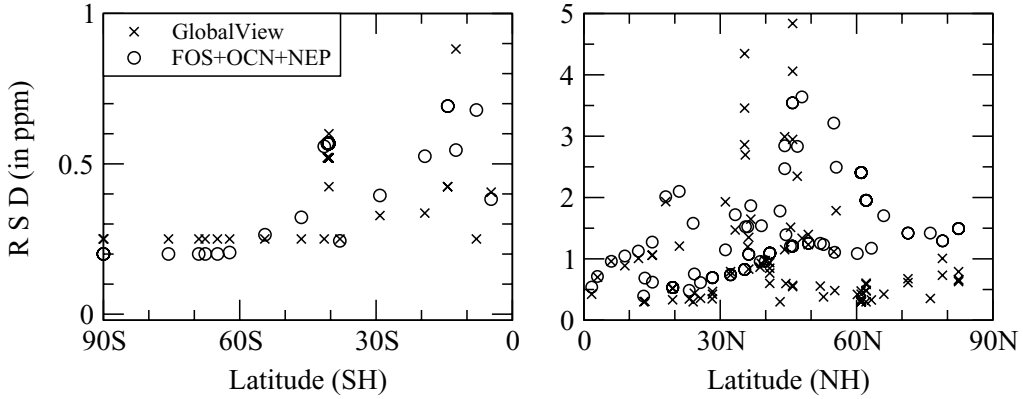

Fig. 2. Comparison of GlobalView RSDs and NIES/FRSGC global transport model derived RSDs for the stations list in basic set (see Fig. 3d for station locations).

The benefit of using a statistically large number of transport models in the network design of CO_2 observations to reduce the flux estimate uncertainty and check robustness of network design is the major focus of this section. Some of the model-specific features and their influence on network design are also studied.

3.1. *Model specific networks*

Figures 3a–c show the network extensions obtained by the IO for the individual transport models (five on each panel). The station locations in the basic set and 15-model ensemble network is shown in Fig. 3d. The network extensions for the individual models suggest that Africa and South/Tropical America (for reference, cf. Fig. 1 for the names and locations of the TransCom-3 inverse model regions) are the most poorly constrained regions in our inverse modeling framework: up to 8 out of 14 new network stations were positioned in these two continents (Table 2). The other regions that require more observations are Temperate Asia, Tropical Asia, Boreal North America, Boreal Asia and South Atlantic ocean. By establishing new stations in these regions the average of flux estimate uncertainties of the inverse model regions could be reduced. This also means that there may be regions that are loosely constrained, but a new station in that region would not lead to a significant improvement in the flux estimates, possibly due to large data error (C_D). Earlier studies by Gloor et al. (2000) and

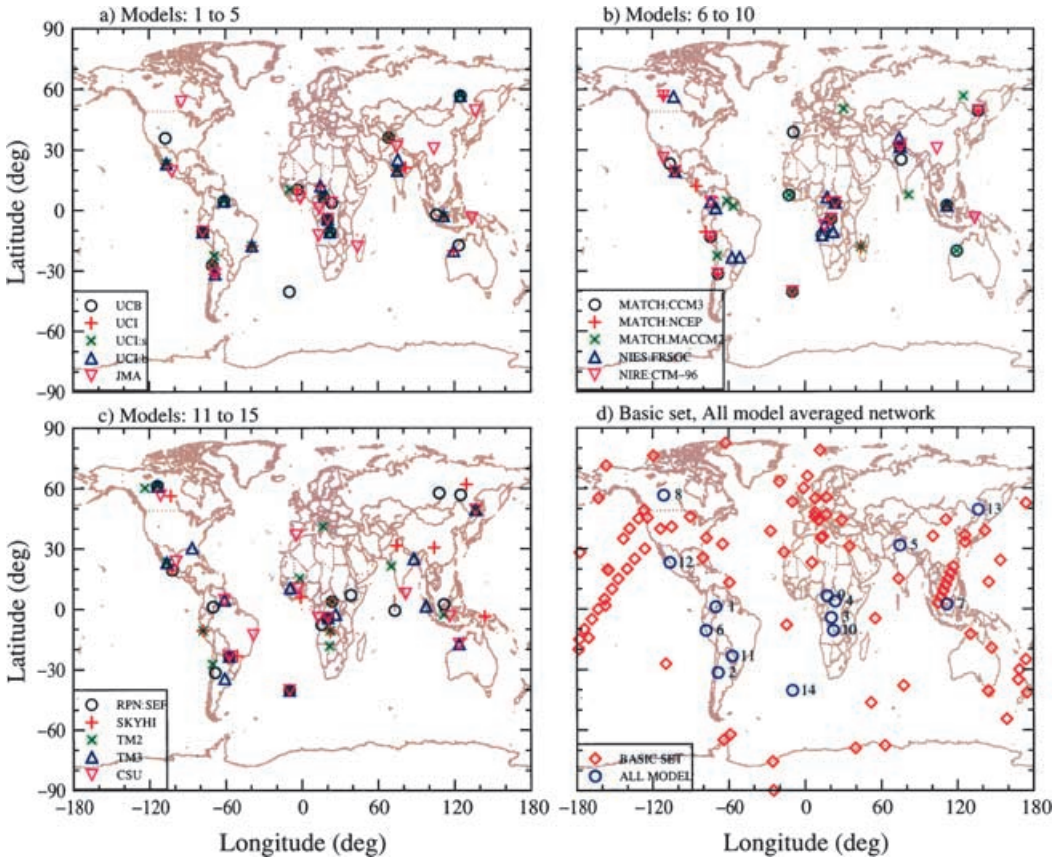

Fig. 3. Station networks for measuring surface CO_2 concentration as obtained by using different models simulated response functions (G): (a) models 1–5, (b) models 6–10 and (c) models 11–15. The model names corresponding to these numbers are given in Table 1. The 115-station basic set (GlobalView, red symbols) and all-model averaged optimal network extended by 14 new stations (blue symbols) are also shown (d). The numbers associated with the symbols are to show the entry sequence of a new station into the basic set.

Table 2. *Summary of regional distribution of the new network stations (first 14) as identified by the individual models and model ensemble*[a]

Region name	Model number 1	2	3	4	5	6	7	8	9	10	11	12	13	14	15	Score -	Ens. net.
L01: Boreal N. America	0	0	0	0	1	0	1	0	1	1	1	1	2	1	1	0.7	1
L02: Temperate N. America	1	1	1	1	1	1	1	1	1	1	1	1	1	1	1	1.0	1
L03: Tropical America	2	1	2	2	1	1	2	2	2	3	1	1	1	2	2	1.7	2
L04: South America	1	3	3	2	1	1	2	1	2	1	2	2	1	2	2	1.7	2
L05: Tropical Africa	3	3	2	2	3	2	2	2	2	1	2	2	2	1	1	2.0	2
L06: South Africa	2	1	2	2	3	2	2	2	3	2	2	2	2	2	2	2.1	2
L07: Boreal Asia	1	0	1	1	1	1	1	1	0	1	2	1	1	1	1	0.9	1
L08: Temperate Asia	1	3	2	3	2	2	1	1	2	2	1	2	1	1	1	1.7	1
L09: Tropical Asia	1	1	1	1	1	1	1	1	1	1	1	1	1	1	1	1.0	1
L10: Australia	1	1	0	1	0	1	0	1	0	0	0	0	0	1	1	0.5	0
L11: Europe	0	0	0	0	0	1	0	1	0	0	0	0	1	0	1	0.3	0
O08: South Atlantic	1	0	0	0	0	1	1	1	0	1	1	1	1	1	0	0.6	1

[a]Score is defined by number of stations/region/model.

Patra and Maksyutov (2002) have also highlighted the need for establishing new measurement sites in the same geographical regions. Therefore, the results are fairly consistent under different network optimization approaches and different experimental setups. The positions of the new station locations are decided based upon sparse data coverage within a particular region and at locations with low C_D and high G values, since this reduces the source estimate uncertainty most efficiently. For example, to constrain the Boreal Asian flux estimate a station is recommended close to the Pacific coast of Siberia, i.e. in the Southeastern corner of this region where C_D values are substantially lower than in the central Boreal Asia. Also the source signal G is higher in the areas located down-wind of a region centre. Sometimes it is also noticed that a few models choose this representative station to be positioned in the Boreal North America (cf. Figs. 3a–c). The inverse model flux uncertainties for Boreal Asia or Boreal North America are correlated, since the regions are connected via atmospheric transport, and their total flux uncertainty is lower than each of them individually. In this case the benefit of adding a new observation point to either of the regions is comparable. This leads to some scatter in placing a station in either regions by different models (Table 2). Unlike in Boreal Asia or Boreal North America, we do not see new stations in the European outflow region. This can be attributed to higher data variability over the continent, which leads to a smaller flux uncertainty reduction by the observations in this area. For the South and Tropical Africa, IO selects stations in the area of maximum regional signal. In Tropical America, the proposed stations are located in the Northern and Eastern part, and those for South America are positioned in the region centre of maximum signal as well as in the East coast region of relatively weak signal accompanied by very low C_D.

In general, there is a lot of similarity between the networks produced with different individual transport models and that by using the model ensemble (see Table 2 for details). The extended networks using separate model simulations indicate that the same regions require more observations for better surface source estimation, with minor differences in the relative importance of particular sites. The good agreement originates in the similarity in pattern of regional source signals simulated by the transport models. The differences in the optimized networks can be attributed not only to differences in model transport but also to model resolution and interpolation of the gridded response functions to station locations. As in the basic TransCom-3 protocol, the simulated signals at grid points nearest to the stations were taken as concentrations at the sites, leading to scatter in the assumed station location. The simulated data variability C_D, however, was produced only with the NIES/FRSGC model, which has a finer grid, and this causes some phase mismatch between the horizontal distribution of G and C_D when used with coarser grid models in areas of sharp signal gradients. For example, such an effect is evident on the area adjacent to Chile's coastline, where some models place the station closer to the coast than others. We have also seen that the gross features in C_D distribution do not change significantly from model to model. The C_D derived from high-frequency data variability for the stations in the basic set show a good correlation (with a coefficient of about 0.8) among the transport models.

3.2. Ensemble network

Next we use the models together to estimate an average flux estimate uncertainty and perform an IO calculation to find an optimally extended network. Unlike for the model-specific networks, we have used the average flux estimate uncertainties over all models and regions to find the impact of candidate stations on the inverse model results. This network is also shown in Fig. 3d (open circles), and is referred to as the 'ensemble network'. A consensus optimal network is found for the model ensemble, which also consistently positions the new CO_2 measuring stations in the poorly constrained regions of high flux estimate uncertainty. However, some differences in the locations of the stations are seen, the station in South America (ranked 2) being the most prominent one. A detailed look at the vertical and horizontal cross-sections of the signal structures simulated by the transport models suggest that the positioning of station 2 by the model ensemble is uncertain and is associated with a mismatch in the horizontal resolution of the transport models. The models simulate a steep gradient in the signals across the Andes mountain range. The model simulated source signal is weak on the Chilean side and stronger on the Argentinian side. Thus the NIES model places the network station in the region interior while the model ensemble places it on the Chilean side. The majority of the University of California (UC) models favour the coastal location, which corresponds to the signal from (53°W, 26°S) because of different horizontal resolution of the models.

3.3. Uncertainty reduction

Figure 4 shows the variations of average regional source estimate uncertainties, defined as

$$\Sigma = \sqrt{\frac{1}{n}\sum_{i=1}^{n} C_S(i,i)}$$

in Gt C yr^{-1} per region (n is the number of inverse model regions), with varying network size. The changes in Σ are fairly uniform over the different models with the number of CO_2 observation stations. The model-averaged value of Σ is rapidly reduced from $\sim$0.53 Gt C yr^{-1} per region, estimated with the GlobalView basic set of 115 stations, to about 0.32 Gt C yr^{-1} per region by introducing 10–15 new observation stations. Further decreases in C_S reach a plateau at about 0.26 Gt C yr^{-1} per region after about 20 additions. On the contrary, the basic set could be reduced, without Σ deteriorating significantly (less than 5%), to about 75 stations if the observational sites are positioned optimally in the inverse modeling perspective for minimizing Σ only (not shown). Since the inverse model setting has quite a coarse horizontal resolution, we find that some of the regions have redundant CO_2 observations. It should be made clear that the intention of this exercise is not to suggest a reduction in CO_2 observations from the same or closely located sites, but to compare the effectiveness of the network extension against the present CO_2 measurement network used in inverse modelling. In fact, overlapping measurements from some sites are strongly recommended in order to keep the inter-laboratory systematic biases under control, which arise mainly due to the calibration offsets and their drift with time (Masarie et al., 2001). Apart from this, the optimal network extension changes rapidly as the resolution of the inverse model

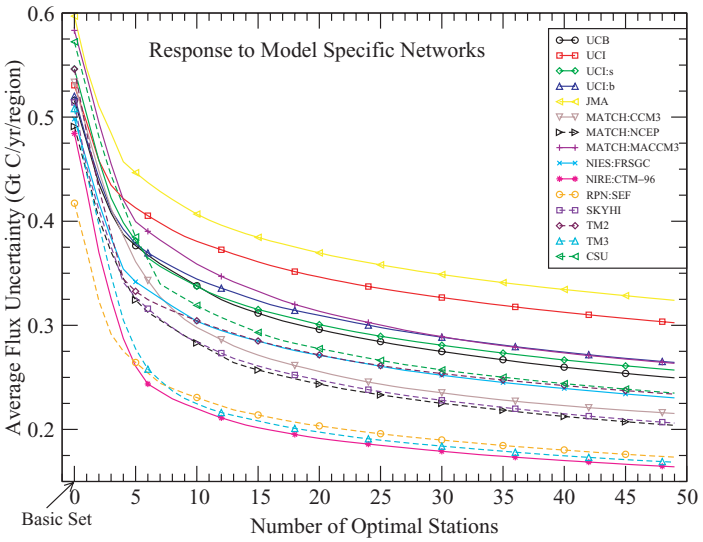

Fig. 4. Variations in average regional flux uncertainty with the additional CO_2 measurement stations obtained for each model by IO. The legend indicates the primary model names and the model variants.

is increased (Gloor et al., 1999). However, it is not an easy task to increase the spatial resolution considering the known deficiency of the present observational network for CO_2. Theory suggests that about 10 randomly located surface observations per region are needed to keep the regional flux uncertainties at a level of 0.1 Gt C yr^{-1} per region (Gloor et al., 1999). For a small network, Gloor et al. also showed that optimal networks are many times more efficient than random networks in constraining flux uncertainties for a 17-region source inversion case. The factors are estimated to be about 10, 4 and 1.25 times for worldwide networks with 40, 80 and 160 stations, respectively.

3.4. *Stability of the networks*

As seen from eq. (3), the scaling of C_D has a direct effect on the flux estimate uncertainty. The implications of choosing different 'effective' data uncertainty (D_u; where $C_D = D_u^2$) maps on the optimal network extension is illustrated in Fig. 5. We have shown the networks for two distinct cases: using averaged value of flux uncertainties from (1) the NIES/FRSGC model and (2) all models with three different D_u maps (D_u = 0.5 ppm, D_u = RSD and $D_u = 2 \times$ RSD) for the candidate stations. The networks corresponding to the use of different D_u values differ significantly from one another. There are several interesting changes when uniform D_u values (0.5 ppm) are used in contrast to using D_u = RSD. First, new stations were positioned in coastal regions in Temperate North America and Tropical/South America using model derived RSDs (circles), but the new stations move inland using uniform D_u (plus symbols). When uniform D_u values are used the new stations are shifted towards the stronger downwind regions in Boreal and Temperate Asia; the station in northern India is moved to eastern China, while the Troickoe station (49°N, 137°E) is moved to Yakutsk (62°N, 129°E) with a much higher priority. These changes are not surprising considering that new preferences are located where the signal strength is larger, but while the supplied D_u values are as low as that in the other parts of the globe. Since the source signal is stronger in the preferred regions and D_u is low, we find a sharper gradient in Σ with the increase in observational network size (Figs. 5c and d). On the contrary, when $D_u = 2 \times$ RSD is used, we find that most of the 14 optimal stations are concentrated in the tropical regions, and the reduction in Σ becomes much slower compared to the other two cases for data uncertainty models. By assigning larger D_u values to the atmospheric CO_2 data, more observations are needed to constrain the regional flux uncertainties. Also, the lowest possible Σ is raised to about 0.35 Gt C yr^{-1} per region for $D_u = 2 \times$ RSD from those of 0.26 and 0.18 Gt C yr^{-1} per region, respectively, for the ensemble networks with 49 optimal stations using D_u = RSD and D_u = 0.5 ppm. Hence, it is suggested that the

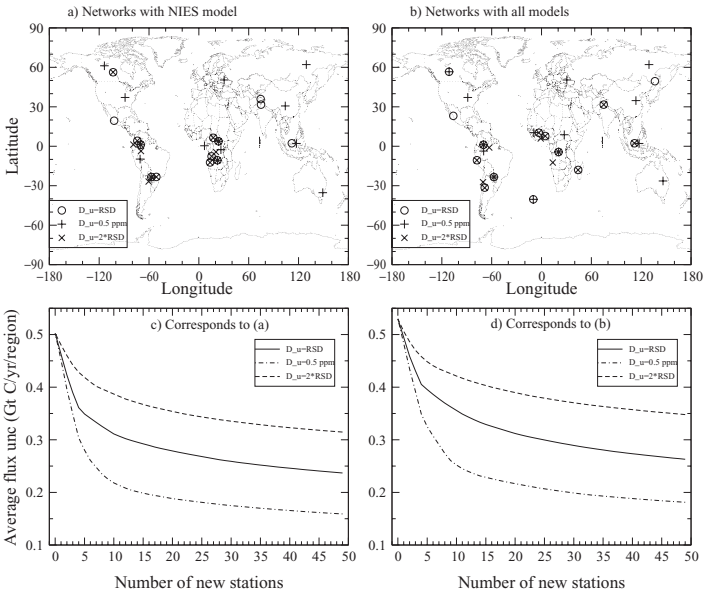

Fig. 5. The effect of using different C_D values on optimal network extension in comparison to those used in Fig. 3. Panels (a) and (b) show the optimal stations by using the NIES/FRSGC model and model ensemble, respectively. Corresponding variations in average flux uncertainties are shown in panels (c) and (d). It could be noted that lower (higher) flux estimates are achieved when lower (higher) C_D values are assigned to the candidate stations.

locations of new stations require a balance between the surface source signal strength and atmospheric data variability.

The robustness of the resulting networks was checked by comparing the reduction in Σ from each model with that for the single ensemble network. The results are shown in Fig. 6a. The general features observed are similar to those shown in Fig. 4. However, a careful examination of the results reveals a number of interesting model-to-model differences. In Fig. 6b the difference between the Σ obtained for model specific networks and the ensemble network is shown. Most models are sensitive to the location of the first few additional stations, suggesting that the transport mechanism, in particular the vertical mixing, of some models are quite different in the tropical region. More discussion on the transport model disparity will be given in the next subsection. Another interesting point is the convergence of the uncertainty reduction after adding 17–20 stations to the existing network. The differences in Σ between the model-specific networks and the ensemble network agree within 20% (equivalent to a spread of about 0.017 Gt C yr^{-1} per region) for all the models. This suggests that differences in the transport models become less important when the network extension is large enough to saturate the flux uncertainty reduction. After adding about 15 stations to the basic observation network, all the inverse model regions in the tropics have at least two stations. Therefore, the results of network design studies can be significantly model-dependent in a scenario where a large number of regional source estimations are underdetermined. In agreement with the small optimized networks (∼40 stations globally for 17 region source inversion) of Gloor et al. (1999), this study indicates that only a few stations per region are needed to keep the flux estimate uncertainty around 0.3 Gt C yr^{-1} per region.

3.5. *Model-to-model differences*

Further analysis of the differences in CO_2 measurement network design between models are made by comparing Σ after adding six tropical stations to the basic set with the average of regional source signals near the surface. Two sets of tests are conducted here by sampling signals (1) at the ensemble network stations, and (2) at the central part of the TransCom-3 regions, where the signal strength is assumed to be the strongest. The results are shown in Figs. 7a and

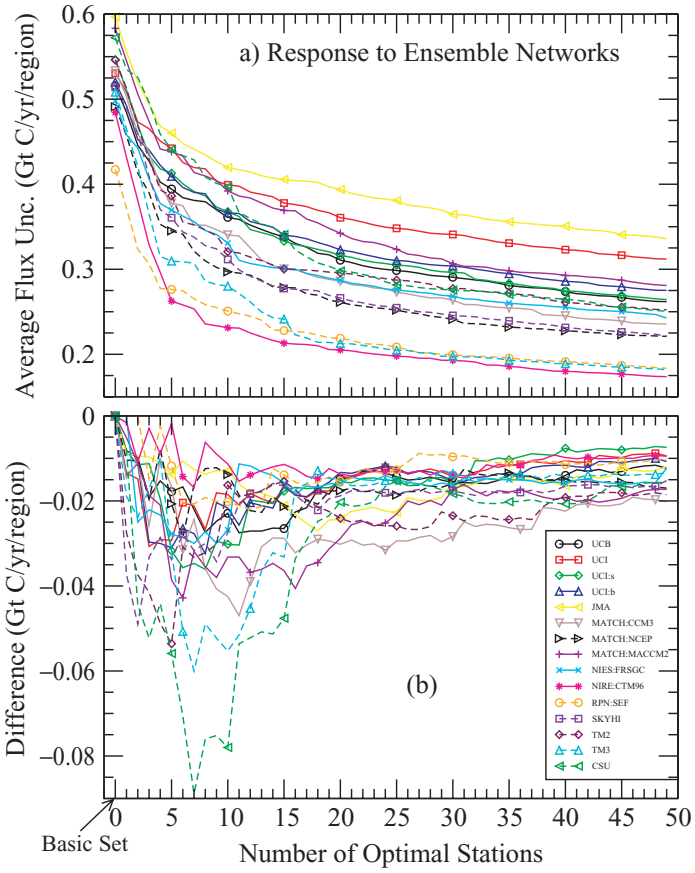

Fig. 6. The upper panel (a) is the same as Fig. 4, but with the ensemble network stations used in place of the model-specific optimal stations. The lower panel (b) is the difference between Figs. 6a and 4.

b, respectively. The vertical profiles of signals show that there is a significant difference between models in transporting the regional source signal near the surface in low-latitude areas (not shown here). Stronger surface-level signals can be related to a lower rate of vertical mixing in the lower troposphere. This difference has not been addressed explicitly before in model validation or calibration studies (such as Jacob et al., 1997 for radon; Denning et al., 1999 for SF_6), because there is a lack of reference tracer observations over the continental tropics, and thus vertical mixing in the lower troposphere in the models is not well constrained. We speculate that the difference originates in the values of effective planetary boundary layer (PBL) height and the way mixing in the PBL connects to vertical transport in the middle troposphere. We find that the model efficiency in constraining the sum of regional flux uncertainties is related to the average surface signal over five regions (L03, L04, L05, L06 and L08). The compact relationship shown in Fig. 7 reveals clearly that models with strong surface level signals over tropical continents provide lower flux uncertainty with the extended network in both cases.

An important implication for transport model design is that vertical mixing and tracer transport in the tropics has to be studied in further detail to provide confident regional flux estimates from CO_2 observational data in low-latitude continental areas, once observations become available.

3.6. *Spatial Structure of* Σ *reduction*

In order to better understand the spatial structure of Σ associated with the candidate stations and its

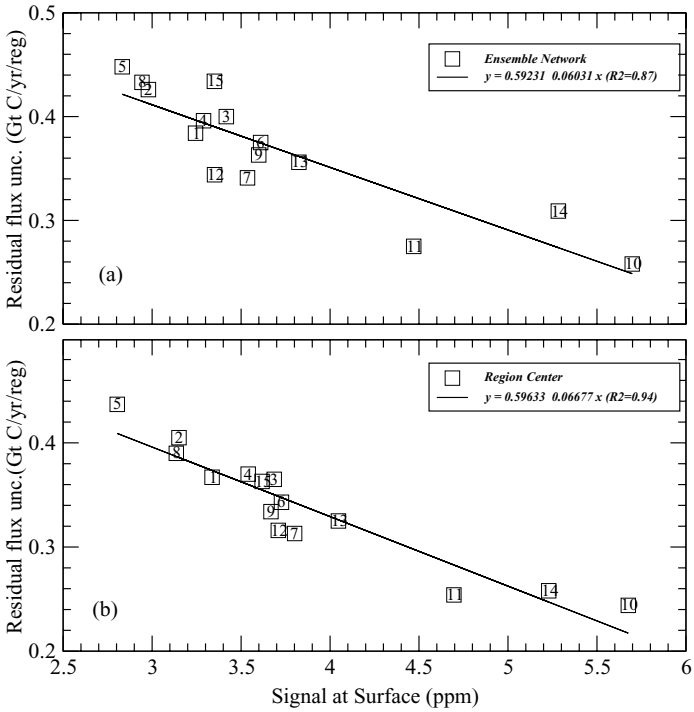

Fig. 7. The average signal of regional sources plotted vs. Σ after adding first six ensemble network stations (a). In the lower panel (b) signals are sampled near the centre of each TransCom-3 regions. For (a) and (b) residual Σ values are taken from Figs. 4 and 6a, respectively. The annotated numbers with each symbol indicate the transport numbers. Compact relations are obtained in both the cases as shown by the straight lines with high correlation coefficients (see legends).

change with the size of the network we first define a station ranking. The initial ranking is calculated by the difference between Σ with the basic set with or without the *i*th candidate station and are expressed in Mt C yr^{-1} per region. Station rankings with the basic network and with five additional stations are shown in Figs. 8a and b, respectively. This ranking was done only with the response functions *G* produced by the NIES/FRSGC model to ensure consistency between the horizontal grid and C_D. It is clear that most of the 446 candidate stations (before any extension) are ranked very high (values exceeding 50) if they are located in South America and Africa (Fig. 8a). However, the picture changes rapidly after optimal extension of the basic set. For example, after introducing an additional five stations, those with a two-digit ranking are seen only rarely (Fig. 8b), and a station in northern India (Amritsar; 32°N, 75°W) scores the highest rank. In other words, Amritsar ranks sixth in this study. It is also important to note that the ranking is dynamic, i.e., with each increment of the basic set the rankings are remapped. For instance, once a new station is introduced in Tropical America (Mitu; 1°N, 70°W), the ranking of the stations around it reduces in the following step and thus the next station is selected from Africa (Dilolo; 11°S, 22°E), even though this was ranked lower than another station in South America (Equals; 4°N, 74°W) in the first step.

We have also tested the extended network of candidate sites by adding elevated levels such as at 1000 and 3000 m altitude. The results do not show that there is much advantage to elevated sampling over surface level sampling, which is understandable as surface source signals decrease faster than noise (variability) with altitude. It should be noted that the use of upper tropospheric measurements on board commercial airliners flying between Tokyo and Sydney has an impact on reducing the flux uncertainties, particularly for regions in the Asian subcontinent (Maksyutov et al., 2003). However, a justifiable conclusion of comparative usefulness of elevated sampling from aircraft or

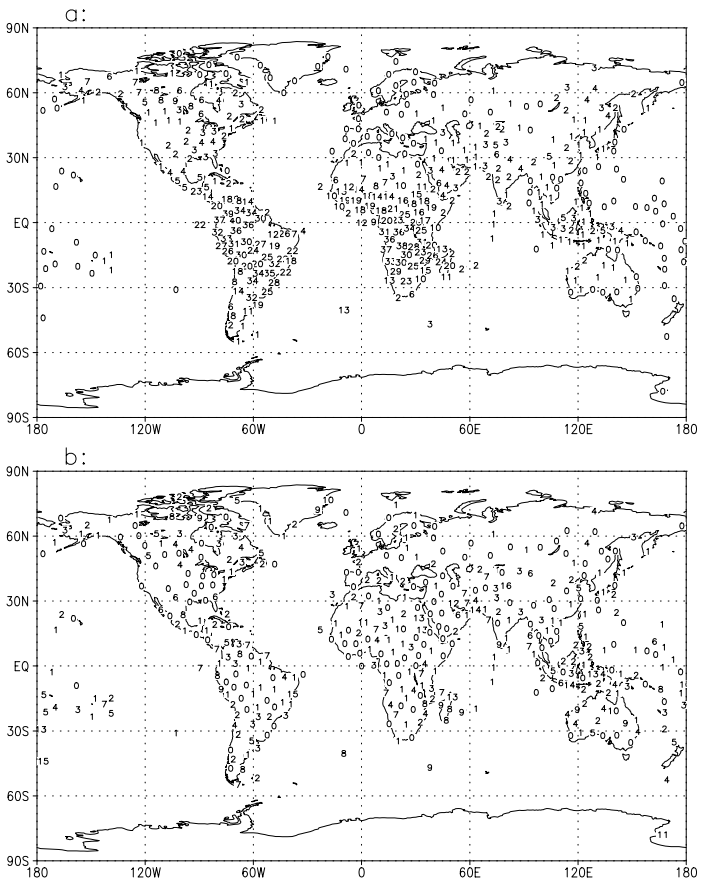

Fig. 8. Rankings of all the candidate stations in terms of their contribution to the reduction of average flux estimate uncertainty. For this calculation we have used only the NIES/FRSGC model simulations. The upper panel (a) shows the ranks at the beginning of the IO procedure, and the lower panel (b) depicts the distribution (much uniform) after adding five stations at the optimal locations.

mountain sites can only be drawn after taking into the account all the components in the signal-to-noise ratio. In particular, the diurnal variability and daily change of the surface fluxes should be taken into account together with a proper sampling protocol for time-independent inversion of annual mean concentration.

4. Conclusions

A detailed analysis of the present CO_2 measurement network has been carried out with the help of simulations from 15 global tracer transport models within an inverse model framework. Based on the incremental optimization technique and using 15 transport model results, we have analysed optimal extensions of the present CO_2 observation network. The average uncertainties in the regional flux estimates are reduced from about 0.53 Gt C yr^{-1} per region to 0.36, 0.32, 0.28 or 0.26 Gt C yr^{-1} per region after adding 5, 10, 15 or 20 new stations to the basic set, respectively. Both rankings of the candidate stations, in terms of reduction in average flux estimate uncertainty, and optimal network design suggest that South and Tropical America, Africa, Boreal North America, Temperate and Boreal Asia and Tropical Asia are the least well constrained regions under this particular inverse modeling framework. A sensitivity study of network extension with three different data uncertainty models indicates that regions with high surface source signal and low data uncertainty are the most preferable sites for new measurements. These regions also have large source

estimate uncertainties at present. The multi-model approach to this network design study also indicates that a robust network will have to be sufficiently large (by about 20 more optimally located stations) to constrain the regional surface sources independent of the differences among transport models. It is also noted that models with larger signals near the ground predict a larger reduction of the regional and global flux estimate uncertainty.

5. Acknowledgements

We thank T. Nakazawa and M. Ishizawa for useful discussions and help with the curve fitting program. PKP acknowledges constructive comments from Roger Francey, Ralph Keeling, Pieter Tans and James White during the WMO/IAEA meeting in Tokyo. The comments and suggestions from three anonymous reviewers have greatly helped to improve the quality of the manuscript. Thanks are also due to Oliver Wild for helping us with the English. The support of H. Akimoto for conducting this research is appreciated. The TransCom-3 work was made possible through support from the National Science Foundation (OCE-9900310), the National Oceanic and Atmospheric Administration (NA67RJ0152, Amend 30) and the International Geosphere Biosphere Program/Global Analysis, Interpretation and Modeling Project.

REFERENCES

Bousquet, P., Peylin, P., Ciais, P., Ramonet, M. and Monfray, P. 1999. Inverse modeling of annual atmospheric CO_2 sources and sinks, 2. Sensitivity study. *J. Geophys. Res.* **104**, 26 179–26 193.

Ciais, P., Tans, P. P., Trolier, M., White, J. W. and Francey, R. 1995. A large northern hemisphere terrestrial CO_2 sink indicated by the $^{13}C/^{12}C$ ratio of atmospheric CO_2. *Science* **269**, 1098–1102.

Denning, A. S., Holzer, M., Gurney, K. R., Heimann, M. and coauthors. 1999. Three-dimensional transport and concentration of SF_6: A model intercomparison study (TransCom-2). *Tellus* **51B**, 266–297.

Enting, I. G., Trudinger, C. M., Francey, R. J. and Granek, H. 1993. Synthesis inversion of atmospheric CO_2 using GISS tracer transport model. *Aust. Div. Atmos. Res. Tech. Pap.* **29**, 1–44.

Fan, S.-M., Gloor, M., Mahlman, J., Pacala, S., Sarmiento, J. L., Takahashi, T. and Tans, P. P. 1998. A large terrestrial carbon sink in North America implied by atmospheric and oceanic carbon dioxide data and models. *Science* **282**, 442–446.

Francey, R. J., Tans, P. P., Allison, C. E., Enting, I. G., White, J. W. C. and Trolier, M. 1995. Changes in oceanic and carbon uptake since 1982. *Nature* **373**, 326–330.

GLOBALVIEW 2000. Cooperative Atmospheric Data Integration Project – Carbon Dioxide. CD-ROM, NOAA CMDL, Boulder, Colorado (anonymous FTP to ftp.cmdl.noaa.gov, path: ccg/CO2/GLOBALVIEW).

Gloor, M., Fan, S., Pacala, S., Sarmiento, J. and Ramonet, M. 1999. A model-based evaluation of inversions of atmospheric transport, using annual mean mixing ratios, as a tool to monitor fluxes of nonreactive trace substances like CO_2 on a continental scale. *J. Geophys. Res.* **104**, 14 245–14 260.

Gloor, M., Fan, S., Pacala, S. and Sarmiento, J. 2000. Optimal sampling of the atmosphere for purpose of inverse modeling: A model study. *Global Biogeochem. Cycles* **14**, 407–428.

Gurney, K., Law, R. M., Denning, A. S., Rayner, P. J. and coauthors, 2002. Towards more robust estimates of CO_2 fluxes: control results from the TransCom3 inversion intercomparison. *Nature* **415**, 626–630.

Gurney, K., Law, R. M., Denning, A. S., Rayner, P. J. and coauthors. 2003. Transcom 3 CO_2 inversion intercomparison: 1. Annual mean control results and sensitivity to transport and prior flux information. *Tellus* **55B**, in press.

Jacob, D., Prather, M. J., Rasch, P. J., Shea, R.-L. and coauthors. 1997. Evaluation and intercomparison of global transport models using ^{222}Rn and other short-lived tracers. *J. Geophys. Res.* **102**, 5953–5970.

Kaminski, T., Rayner, P. J., Heimann, M. and Enting, I.G. 2001. On aggregation errors in atmospheric transport inversions. *J. Geophys. Res.* **106**, 4703–4715.

Maksyutov, S. and Inoue, G. 2000. Vertical profiles of radon and CO_2 simulated by the global atmospheric transport model. In: *CGER supercomputer activity report*. CGER/NIES-I039-2000, Vol. 7, 39–41.

Maksyutov, S., Machida, T., Mukai, H., Patra, P. K., Nakazawa, T., Inoue, G. and coauthors. 2003. Effect of recent observations on Asian CO_2 flux estimates with transport model inversions. *Tellus* **55B**, this issue.

Masarie, K. A. and Tans, P. P. 1995. Extension and integration of atmospheric carbon dioxide data into a globally consistent measurement record. *J. Geophys. Res.* **100**, 11 593–11 610.

Masarie, K. A., Langenfeld, R. L. and coauthors. 2001. The NOAA/CSIRO flask-air intercomparison program: A strategy for directly assessing consistency among atmospheric measurements derived from independent laboratories. *J. Geophys. Res.* **106**, 20 445–20 464.

Nakazawa, T., Ishizawa, M., Higuchi, K. and Trivett, N.B.A. 1997. Two curve fitting methods applied to CO_2 flask data. *Environmetrics* **8**, 197–218.

Patra, P. K. and Maksyutov, S. 2002. Incremental approach to the network design for CO_2 surface source inversion. *Geophys. Res. Lett.* **29**, 0.1029/2001GL013943, 97–1.

Press, W., Teukolsky, S., Vetterling, W. and Flannery, B. 1992. *Numerical recipes*, 2nd edn Cambridge University Press, Cambridge, U. K., 973.

Rayner, P. J., Enting, I. G. and Trudinger, C. M. 1996. Optimizing the CO_2 observing network for constraining sources and sinks. *Tellus* **48B**, 433–444.

Tans, P., Fung, I. and Takahashi, T. 1990. Observational constraints on the global atmospheric CO_2 budget *Science* **247**, 1431–1438.

Tarantola, A. 1987. *Inverse problem theory*, Elsevier Amsterdam, The Netherlands, 605.